Journal of Power Sources 185 (2008) 1079–1085

Contents lists available at ScienceDirect

Journal of Power Sources

journal homepage: www.elsevier.com/locate/jpowsour

Nanowire-based three-dimensional hierarchical core/shell heterostructured electrodes for high performance proton exchange membrane fuel cells

Madhu Sudan Saha[a,1], Ruying Li[a], Mei Cai[b], Xueliang Sun[a,*]

[a] Department of Mechanical and Materials Engineering, The University of Western Ontario, London, Ontario N6A 5B9, Canada
[b] General Motors Research and Development Center, Warren, MI 48090-9055, USA

ARTICLE INFO

Article history:
Received 24 June 2008
Received in revised form 22 July 2008
Accepted 23 July 2008
Available online 31 July 2008

Keywords:
Electrocatalysis
Oxygen reduction reaction
Polymer electrolyte membrane fuel cells
SnC nanowires

ABSTRACT

In order to effectively utilize expensive Pt in fuel cell electrocatalyst and improve the durability of PEM fuel cells, new catalyst supports with three-dimensional (3D) open structure are highly desirable. Here, we report the fabrication of a 3D core/shell heterostructure consisting tin nanowire core and carbon nanotube shell (SnC) grown directly onto fuel cell backing (here carbon paper) as Pt catalyst support for PEM fuel cells. Compared with the conventional Pt/C membrane electrode assembly (MEA), SnC nanowire-based MEA shows significantly higher oxygen reaction performance and better CO tolerance as well as excellent stability in PEM fuel cells. The results demonstrate that the core/shell nanowire-based composites are very promising supports in making cost effective and electrocatalysts for fuel cell applications.

1. Introduction

Proton exchange membrane (PEM) fuel cells are considered to be the most promising alternative energy devices in transportation, stationary and portable applications due to their immobilized electrolyte, high efficiency, high energy density and zero-noxious emission [1]. However, several challenges such as hydrogen fuel infrastructure, fuel cell stack durability, and cost issues need to be overcome before the commercialization of PEM fuel cells [2,3]. Another critical effect associated with low operational temperature PEM fuel cells is the low tolerance to fuel impurities, e.g., CO in the hydrogen steam. For example, CO content as low as 20 ppm in the fuel steam will result in a significant loss in the cell performance [4]. To overcome the material barrier of electrocatalysts, the discovery of new high-activity electrocatalyst materials with reduced precious metal content is necessary [5]. There are two primary approaches that may be used to reduce the Pt metal requirement in PEM fuel cells: (i) reduction of the mass-transport losses particularly at high current densities by improving diffusion media and improving electrode structures and/or (ii) improvement of catalyst activity and catalyst utilization [6]. The exploration of new catalyst supports with improved fuel cell performance and electrode structure, better durability and higher tolerance to CO is highly desirable for both approaches [7].

Carbon black (Vulcan XC-72) is commonly used as the support for Pt catalysts in the state of the art PEM fuel cell electrocatalysts [8]. Despite its high surface area and low electrical resistance, current fuel cell electrocatalyst still suffers from low Pt utilization, limited mass-transport capability, and limited electrochemical stability due to the usage of carbon black-based support in the electrode structure [3]. Therefore, carbon nanostructure-based new electrode materials such as carbon nanotubes (CNTs) and carbon nanofibers have attracted significant interests in recent years for improved fuel cell performance due to their unique structure, high surface area, good electronic conductivity, strong mechanical properties and chemical stability [9–15]. Several research groups have reported that CNTs are more resistant to electrochemical oxidation than that of carbon black, with and without Pt on them [16–18]. More recently, 3D structure of CNT-based composite electrode, which involves the growth of CNTs directly on the carbon fibers of a fuel cell backing with subsequent deposition of metal catalysts, was fabricated [19–24]. The unique advantage of this approach is that all the deposited Pt particles are in electrical contact with the external electrical circuit. As a result, much improved Pt utilization was achieved because of the 3D open structure [19,21,22].

Compared with CNTs, nanowires (NWs) are a newer class of one-dimensional (1D) nanomaterials with a high aspect ratio and they have demonstrated unique electrical, optical, mechanical and thermal properties [25–28]. Using NWs, especially metal and metal oxide NWs, as supports for Pt nanoparticles have unique advan-

* Corresponding author. Tel.: +1 519 661 2111x87759; fax: +1 519 661 3020.
E-mail addresses: mssaha@ymail.com (M.S. Saha), xsun@eng.uwo.ca (X. Sun).
[1] Present address: Queen's-RMC Fuel Cell Research Centre, 945 Princess Street, Kingston, Ontario K7L 5L9, Canada.

0378-7753/$ – see front matter © 2008 Elsevier B.V. All rights reserved.
doi:10.1016/j.jpowsour.2008.07.066

tages for practical applications. It has been reported that SnO_2 NWs reveal high catalytic properties and their combination with Pt metal catalyst significantly enhanced the overall catalytic activities [29,30]. Moreover, there is a strong metal-support interaction between Pt nanoparticles and metal oxide surface [31]. Because of these, our interests are to explore the feasibility of using NW supports for Pt-based catalysts in PEM fuel cells and direct methanol fuel cells (DMFCs). In our recent work [32], we grew SnO_2 NWs directly on a carbon paper substrate with subsequent electrodeposition of Pt nanoparticles onto them to form a composite electrode. The Pt nanoparticles supported on SnO_2 NWs exhibited relatively higher electrocatalytic activity for oxygen reduction reaction than that of the Pt nanoparticles supported on carbon black. In another report [33], Pt–Ru nanoparticles deposited on SnO_2 NWs showed considerably higher methanol oxidation mass activity and specific activity as well as higher CO tolerance for methanol oxidation reaction than the one supported on the glassy carbon electrode.

However, the major drawback of metal and metal oxide nanowires is relative poor electrical conductivity and corrosion resistance [34,35]. One of the strategies to improve them is to synthesize nanowires coated with carbon. It has been reported that carbon was coated on Sn or Sn-based oxide nanoparticles to promote their electrochemical performances [36–38]. Morishita et al. [37] reported that the carbon-coated Sn powder gave higher discharge–charge performance in comparison to carbon powder. This higher performance of carbon-coated Sn powder was supposed to be due to the presence of open spaces neighboring to metallic Sn in carbon shell, which could absorb a large volume expansion due to alloying of Li into Sn metal. Read et al. [38] used hard carbon as a diluent in place of the oxides, which could prevent tin agglomeration. Recently, through a one-step chemical vapor deposition method, we have synthesized core/shell nanostructured Sn nanowires encapsulated in amorphous carbon nanotubes directly grown on carbon paper [39]. Here, we report a high performance 3D fuel cell electrode consisting of Pt nanoparticles supported on core/shell heterostructure of Sn nanowires coated with graphitic carbon nanotubes grown directly on fuel cell backing of carbon paper. The Pt nanoparticles supported on carbon-coated Sn nanowires composites were characterized using SEM, XPS and TEM. The catalytic performance was evaluated in a single PEM fuel cell.

2. Experimental

2.1. Growth of carbon-coated Sn nanowires

The synthesis of carbon-coated Sn NWs was carried out by thermal evaporation method. The detailed synthesis procedure has been described previously [39], except different growth temperatures. Here, a higher temperature of 950 °C instead of 900 °C was used, resulting a graphite carbon-coated layer rather than amorphous carbon coating. In a typical procedure, pure commercial grade Sn powders (2 g, 325 mesh, 99.8%) were loaded in an alumina boat (7.5 cm × 1.2 cm) placed at the middle of a quartz tube (1.8 cm inner diameter and 75 cm length) in a horizontal tube furnace. A small piece of commercially available carbon paper (E-TEK, a division of De Nora North America, Somerset, NJ) as substrate for the growth of product was placed beside the metal powder. The reaction chamber was heated to 950 °C rapidly (in about 15 min) from room temperature with an argon flow rate of 200 sccm (standard cubic centimeters per minute) and 2% ethylene gas was introduced during the growth of NWs with flow rate of 200 sccm. Subsequently, the furnace was cooled to room temperature. After the reaction, it was observed that gray dark-like products (thin films) were deposited on the surface of the carbon paper substrates. The resultant nanostructure was denoted as SnC NWs/carbon paper.

2.2. Deposition of Pt nanoparticles on SnC NWs/carbon paper

The deposition of Pt nanoparticles on SnC NWs support were prepared by reduction of Pt precursors with glacial acetic acid as described previously [19]. In a typical procedure, predetermined amount of Pt precursor was added into 25 ml of glacial acetic acid followed by agitation in an ultrasonic bath for 10 min. The SnC NWs/carbon paper were immersed into the solution and then heated at a temperature of 110 ± 2 °C for around 5 h under constant stirring. Afterward, the Pt nanoparticles supported SnC NW/carbon paper (Pt/SnC NW/carbon paper) composites were washed with deionized water and dried at 85 °C over night in a vacuum oven. The Pt loading in the Pt/SnC NW/carbon paper composites was determined by inductively coupled plasma-optical emission spectroscopy (ICP-OES). The morphologies of the composites were characterized by X-ray photoelectron spectroscopy (XPS), scanning electron microscope (SEM) (Hitachi S-2600 N) and transmission electron microscopy (TEM) (Philips CM10). The XPS analyses were carried out with a Kratos Axis Ultra spectrometer using a monochromatic Al Ka source (15 mA, 14 kV).

2.3. Electrochemical measurements

Cyclic voltammetry was conducted at room temperature using an Autolab potentiostat/galvanostat (Model, PGSTAT-30, Ecochemie, Brinkman Instruments) with a three-electrode, two-compartment configuration. Pt wire and a reversible hydrogen

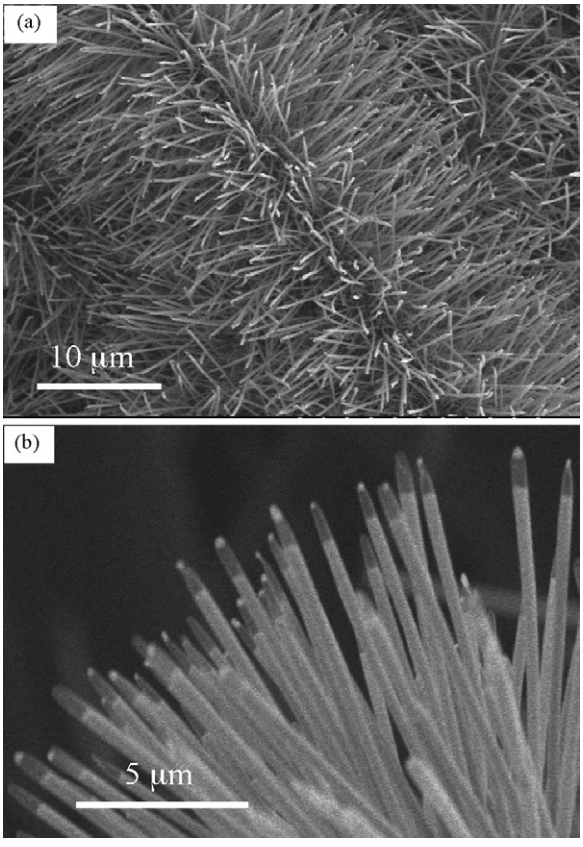

Fig. 1. (a) SEM image showing high coverage of SnC NWs grown on fibers of carbon paper; (b) Higher magnification SEM image showing the tip of nanostructure array.

electrode (RHE) were used as the counter and reference electrodes, respectively. For the measurement of hydrogen electrosorption curves, the potential was cycled between 0.0 and +1.2 V at 50 mV s^{-1} to obtain the voltammograms of hydrogen adsorption in Ar-purged 0.5 M H_2SO_4 aqueous solution. For CO stripping voltammetry, pure CO (99.5%) was purged into solution at a position close to the working electrode for at least 1 h, with the electrode polarized at 0.05 V vs RHE in a fume hood. The electrode was then purged with pure Ar for 1 h under potential control followed by voltammetric stripping.

2.4. Preparation and characterization of MEA

To fabricate membrane electrode assembly (MEA), Pt/SnC NW/carbon paper composite with a Pt loading of 0.21 mg cm^{-2} was used as the cathode. A gas diffusion layer was applied on the backside of the SnC NW/carbon paper composite according to reported method [40]. For comparison, the commercial Pt/C electrocatalyst obtained from E-TEK (30 wt.% Pt on carbon black) was used in the cathode. Regarding preparation of conventional electrode, carbon paper backing was hydrophobically treated with polytetrafluoroethylene (PTFE) to reach a loading of 10 wt.% and then annealed at 350 °C in air. A gas diffusion layer was then applied with the same loadings of PTFE and carbon black as in the Pt/SnC NW/carbon paper composite. A catalyst layer composition of Pt/C catalyst, Nafion solution and iso-propanol was applied on the gas diffusion layer. The ratio of dry Nafion to Pt/C was 1:3 by weight and the Pt loading was 0.20 mg cm^{-2}. The anodes were used commercially available 30 wt.% Pt/C on single-sided ELAT with a Pt loading of 0.5 mg cm^{-2}. The electrode area was 1.0 cm^2 and typical loading of Nafion solution in all electrodes was in the ranges of 0.8–1.0 mg cm^{-2}. Nafion 112 (DuPont Inc., USA) was used as the polymer electrolyte membrane. The MEA was fabricated in-house via hot pressing at 130 °C and 150 psig for 2 min. Polarization curve experiments were carried out a single fuel cell test station (Fuel Cell Technologies, Inc., USA).

3. Results and discussion

Fig. 1 shows the SEM images of the SnC NWs grown on a commercially available carbon paper backing used in fuel cell applications. The carbon paper substrate is made of small graphite fibers with a diameter between 5 and 10 μm (inset in Fig. 1a). It can be observed that the surface of the carbon fibers in the carbon paper was completely covered by a high density of uniform and radically distributed SnC NWs (Fig. 1a). The length of the SnC NWs is in the range of 20–30 μm. Further, close SEM examinations reveal that a dark region, about 1 μm in length, is present on the tips of each nanostructure, separated by the light region as shown in Fig. 1b. TEM images indicate that the dark regions are hollow carbon nanotubes, and the light regions are tin nanowires encapsulated in carbon nanotube, as observed in Fig. 2a.

After the deposition of Pt nanoparticles onto SnC NWs/carbon paper, TEM images reveal that the Pt nanoparticles dispersed homogeneously on the surface of SnC NWs and with average particle sizes of about 2 nm (Fig. 2a–c). Further, a high resolution TEM lattice image in Fig. 2d reveals that the carbon-coated layer is graphite structure with lattice space of 0.34 nm. The typical Pt particles are 2 nm on the surface. The Pt loading in the Pt/SnC NW/carbon paper composites was determined to be 0.21 mg_{Pt} cm^{-2} by ICP-OES.

The electrical contact between SnC NWs and the carbon fibers of carbon paper was investigated by cyclic voltammetry (CV) and

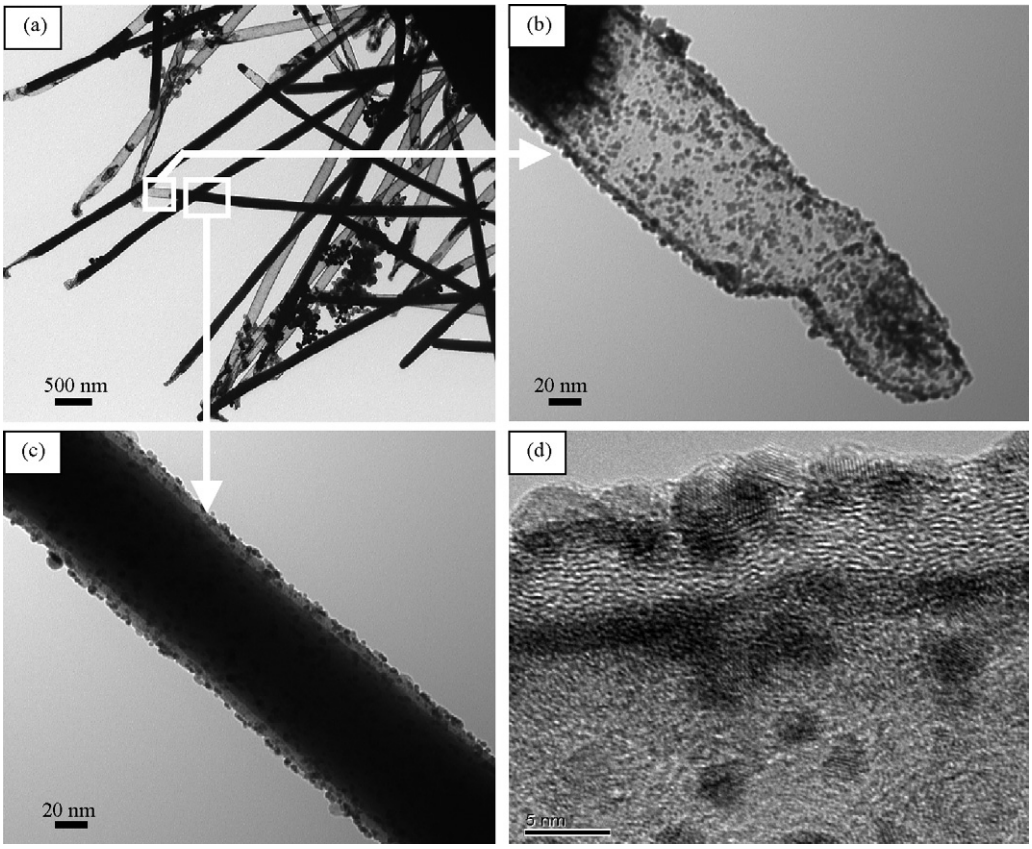

Fig. 2. TEM images of Pt nanoparticles deposited on SnC NWs/carbon paper by chemical reduction with glacial acetic acid: (a) low magnification showing distribution of Pt nanoparticles; (b and c) enlargements of selected sections of image (a); and (d) high resolution TEM image showing individual Pt particles and nanowire lattice fringe.

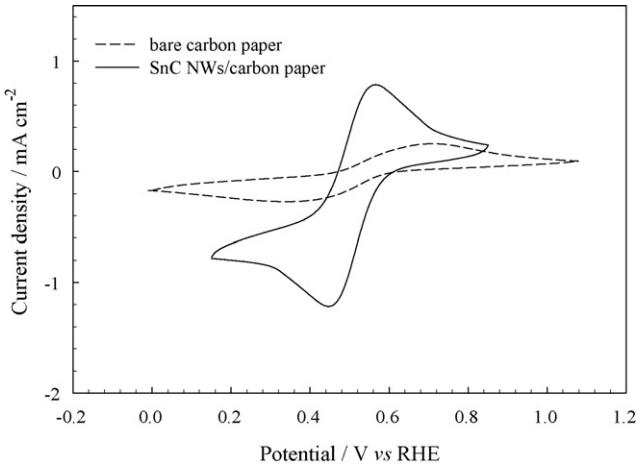

Fig. 3. CVs in a $K_3Fe(CN)_6$ aqueous solution (5 mM $K_3Fe(CN)_6$ + 0.5 M K_2SO_4) of: bare carbon paper and SnC NWs/carbon paper electrode. Potential scan rate: 50 mV s^{-1}. The current density values are with respect to the geometrical area.

shown in Fig. 3. The CV was taken at a bare carbon paper and SnC NWs grown on carbon paper in $K_4Fe(CN)_6^{-3/-4}$ solution. A much higher redox current and a larger surface area were obtained on SnC NWs/carbon paper composite electrode, strongly suggesting that the NWs are electrically connected to the carbon fibers of the fuel cell baking.

The surface oxidation states of Pt nanoparticles deposited on SnC NWs/carbon paper was determined by XPS (Fig. 4) The Pt ($4f_{7/2}$) and Pt ($4f_{5/2}$) peaks are presented at 71.2 and 74.3 eV, respectively, indicating Pt particles in the Pt supported SnC NW/carbon paper composite are zero-valent.

The electrosorption properties of Pt nanoparticles in Pt/SnC NW/carbon paper composite were examined by CV shown in Fig. 5a. For comparison, the commercially available 30 wt.% Pt/C electrocatalyst was also examined under the same conditions. The voltammetric features of Pt/SnC NW/carbon paper composite electrode reveal the typical characteristics of Pt metal [41], with well-defined hydrogen adsorption and desorption peaks as well as oxide formation and reduction peaks in the low and high potential regions, respectively. Fig. 5b shows adsorbed CO (CO_{ads}) stripping voltammograms for the Pt/SnC NW/carbon paper composite along with one of a commercial Pt/C electrode in 0.5 M H_2SO_4 solution at

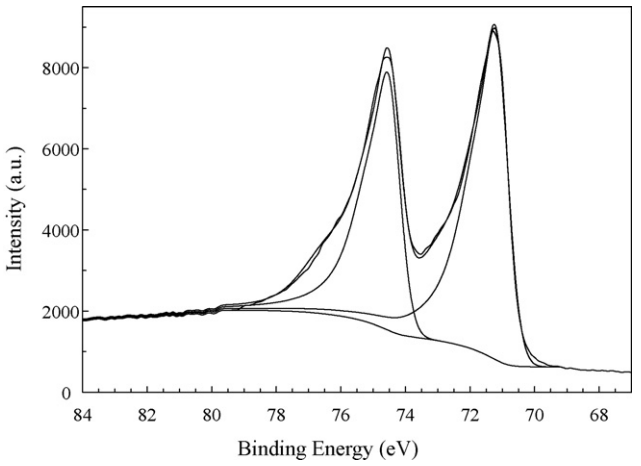

Fig. 4. XPS spectra of SnC NWs/carbon paper after Pt nanoparticles deposited by chemical reduction with glacial acetic acid.

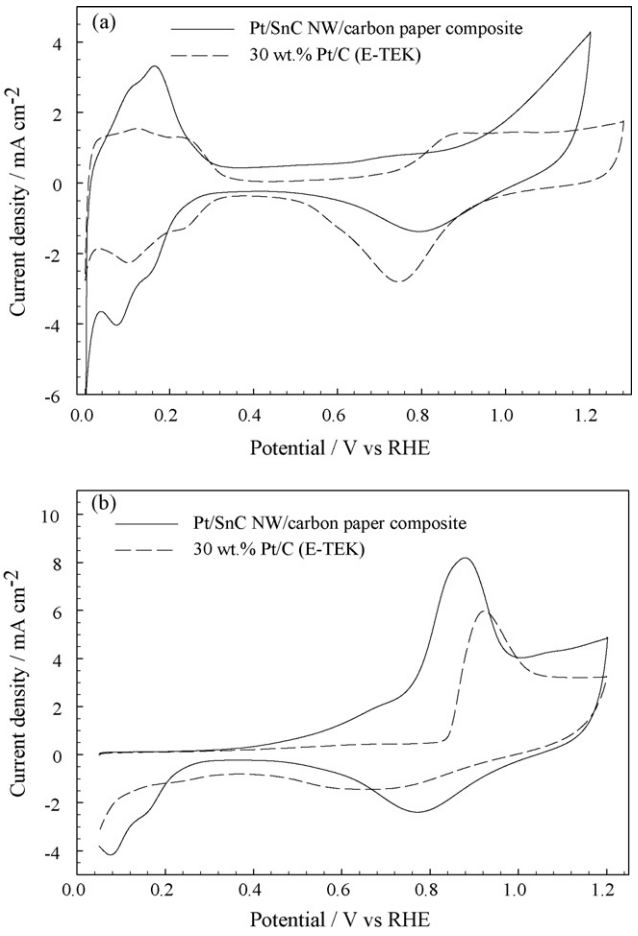

Fig. 5. CVs of Pt/SnC NW/carbon paper composite electrode (a) in the absence and (b) presence of CO in 0.5 M H_2SO_4 aqueous solution at room temperature. Potential scan rate: 50 mV s^{-1}. The CO was absorbed at 0.05 V for 1 h, subsequently, the solution CO was removed by Ar bubbling for 1 h while maintaining the potential at 0.05 V vs RHE. A representative CV of a standard 30 wt.% Pt/C electrode is included for reference. The current density values are with respect to the geometrical area.

a scan rate of 50 mV s^{-1}. CO was purged while holding the potential at 0.05 V vs RHE for 1 h at 25 °C. The observed CO-stripping peak potential of 0.88 V for the Pt/SnC NW/carbon paper composite, which is more negative than the Pt/C electrode under the same conditions (0.93 V). This result indicates the CO_{ads} oxidation becomes energetically more favorable at the Pt/SnC NW/carbon paper composite electrode than the Pt/C electrode. As can be seen in Fig. 5b, the presence of tin in the Pt/SnC NW/carbon paper catalyst allows adsorbed CO to be oxidized at lower potentials compared with Pt/C catalyst. This result is in agreement with the work of Crabb et al. [42], in which the onset potential of carbon monoxide oxidation was found to be lowered due to the addition of a small amount of tin. It was reported that CO-tolerant can be improved by combinations of Pt and oxophilic elements, such as ruthenium, tin, molybdenum, osmium, etc. in binary, ternary or quaternary alloys [43–45]. The role of these additional elements are to promote the electro-oxidation of CO to CO_2 through a spillover process involving OH-species formed on the oxophilic sites and CO adsorbed at the Pt sites, as proposed in the so-called bifunctional mechanism [46]. The specific electrochemical surface areas ($m^2\,g_{pt}^{-1}$) of Pt (sometimes referred to as the real Pt catalyst surface area) were measured from CO_{ads} stripping accordingly to the equation: [47] $A_{EL}(m^2\,g_{pt}^{-1}) = Q_H/(0.42 \times 10^{-3}\,C\,g_{pt}^{-1})$. The specific electrochemical surface areas of the electrocatalysts was also estimated from

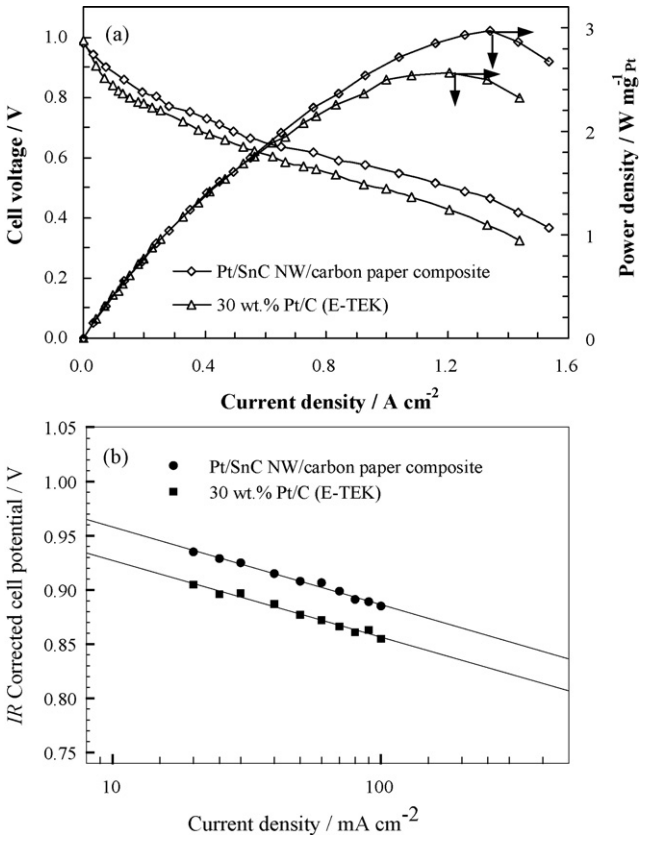

Fig. 6. (a) Comparison of single cell performance of MEAs made with Pt/SnC NW/carbon paper composite (0.21 $mg_{Pt}\,cm^{-2}$) and conventional Pt/C electrode (0.20 $mg_{Pt}\,cm^{-2}$) as cathodes for H_2/O_2 at 80 °C, Nafion 112 membrane, 25/30 psig anode and cathode back pressure, respectively. Anodes were E-TEK gas diffusion electrode with a Pt loading of 0.5 $mg_{Pt}\,cm^{-2}$; (b) Comparison of the iR-free Tafel plots for oxygen reduction reaction.

the integrated charge in the hydrogen adsorption and desorption region of the CVs. Comparison of electrochemically active surface obtained from CO_{ads} and H_{upd} indicate remarkable agreement. The A_{EL} of Pt/SnC NW/carbon paper electrode is 59.3 $m^2\,g_{pt}^{-1}$, which is 46% higher than the commercial Pt/C electrode (40.6 $m^2\,g_{pt}^{-1}$), suggesting an increased Pt utilization of the Pt nanoparticles deposited onto SnC NWs/carbon paper that are in electrical contact with carbon paper. The higher specific electrochemical surface area for the Pt/SnC NW/carbon paper electrode can also be attributed to the effect of the presence of Sn.

Fig. 6a shows the single cell performance of the MEA made with Pt/SnC NW/carbon paper composite electrode as the cathode and standard E-TEK electrode as the anode for H_2/O_2. For comparison, the polarization curve of the conventional MEA made with two E-TEK electrodes is also presented. Polarization characteristics were compared at 80 °C with 25/30 pisg backpressure for the anode and cathode, respectively (100% humidification condition). As seen in Fig. 6a, the MEA made with Pt/SnC NW/carbon paper composite electrode shows higher performance compared to that conventional E-TEK MEA throughout the whole potential range. Comparison of the iR-free Tafel plots for oxygen reduction is presented in Fig. 6b. The mass activity (current density normalized on the basis of Pt loading) at 900 mV (activation-controlled region) for the Pt/SnC NW/carbon paper composite is 308.6 $mA\,mg_{pt}^{-1}$, which is 2.5 times higher than the value of 121.0 $mA\,mg_{pt}^{-1}$ for the Pt/C electrode, indicating a higher activity toward oxygen reduction at Pt/SnC NW/carbon paper composite. This improvement can be attributed to the higher dispersion of Pt nanoparticles on the surface of SnC NWs as well as the unique 3D structure of Pt/SnC NW/carbon paper composite. Moreover, the enhanced performance and power density are achieved at higher current density region using the Pt/SnC NW/carbon paper composite. The improvement at higher current density region clearly indicates a better mass transport for the Pt/SnC NW/carbon paper composite electrode. The power density of a Pt/SnC NW/carbon paper composite electrode and Pt/C electrode, both were normalized to the Pt loading at 0.6 V, were 2.14 and 1.70 $W\,mg_{pt}^{-1}$, respectively, showing an improvement of about 0.44 $W\,mg_{pt}^{-1}$ in power density for the Pt/SnC NW/carbon paper composite electrode.

The stability of SnC NWs on carbon paper (before Pt nanoparticles deposition) was evaluated by immersing the composite electrode in 0.1 M H_2SO_4 solution over a period of 1500 h at 50 °C. After the test, TEM observations of the composite indicate that SnC NWs are still on the surface of carbon fibers with same density, diameter, and length (Fig. 7a). Further TEM inspection shows that both the tin core and carbon shell remain original morphology (Fig. 7b). These results suggest that the adhesion of SnC NWs to the carbon paper is strong and the stability of SnC NWs is high.

In addition, the preliminary stability assessment of electrochemical activity in a single PEM fuel cell using Pt/SnC NW/carbon paper composite cathode was also performed by recording the cell voltage with time (Fig. 8a) and the polarization curves before and after polarizing the fuel cell at a constant current density of 500 $mA\,cm^{-2}$ over a period of 120 h (Fig. 8b). The cell exhibits stable

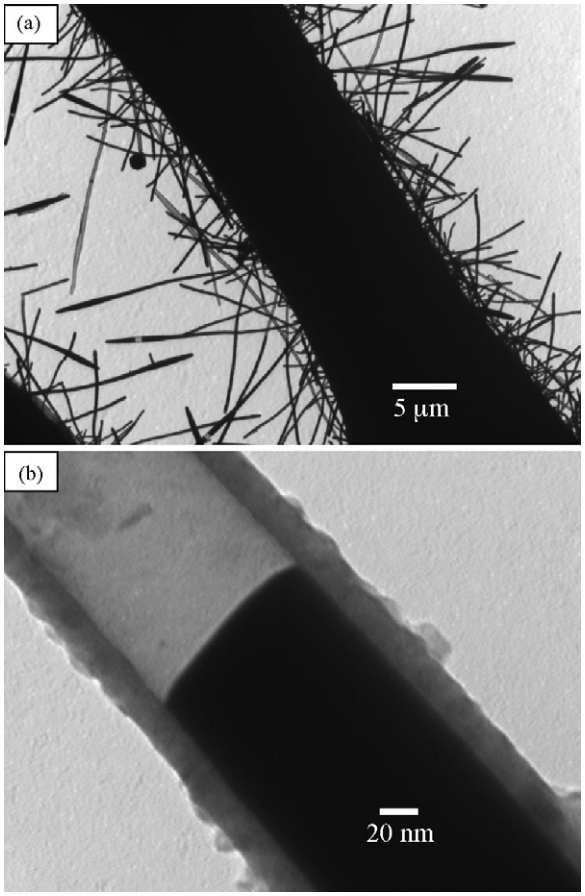

Fig. 7. TEM images SnC NWs/carbon paper after immersing it in 0.1 M H_2SO_4 solution over a period of 1500 h at 50 °C.

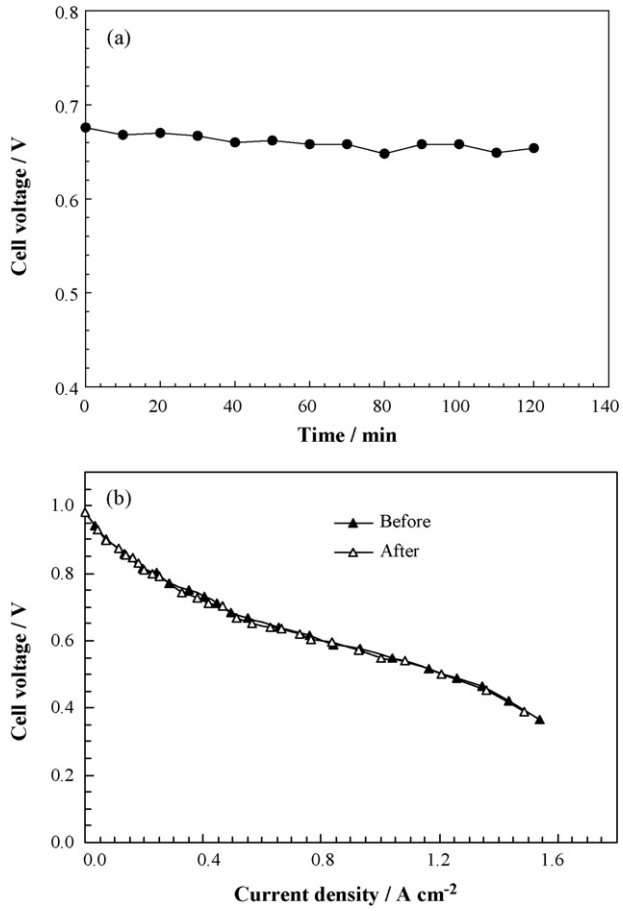

Fig. 8. The stability evaluation of the Pt/SnC NW/carbon paper composite cathode upon polarizing the cell at 500 mA cm^{-2} for 120 h in a single cell PEM fuel cell: (a) cell voltage variation during the time of polarization and (b) steady-state polarization curves before and after polarization. Other experimental conditions are the same as in Fig. 6.

voltage within this test period (Fig. 8a) without any change in the curves before and after polarizing the cell (Fig. 8b), indicating an excellent stability for the Pt/SnC NW/carbon paper composite electrode.

4. Conclusions

In summary, novel Pt/SnC NW/carbon paper composite electrodes were successfully prepared. The produced Pt/SnC NW/carbon paper composite electrodes showed higher specific electrochemical surface area and enhanced tolerance to CO (as evaluated from cyclic voltammetry) than that of the commercial Pt/C electrode. This can be ascribed to the high dispersion of small Pt nanoparticles on the nanowires surface and the effect of Sn nanowires. These composite electrodes exhibited higher electrocatalytic activity for oxygen reduction reaction in a single PEM fuel cell compared to Pt/C electrode. The higher performance is attributed to a 3D open structure of Pt/SnC NW/carbon paper composite and the better utilization of the catalytic particles. The primary durability test result showed that a single PEM fuel cell made with Pt/SnC NW/carbon paper composite as cathode has a good stability at cell working conditions. This study therefore clearly demonstrates the great potentials of using core/shell nanowire-based support for the fabrication of cost effective and durable PEMFC electrodes.

Acknowledgements

This research was supported by General Motors of Canada, Natural Sciences and Engineering Research Council of Canada, Canada Research Chair Program, Canada Foundation for Innovation, Ontario Early Researcher Award and the University of Western Ontario. We are in debt to Dr. Yong Zhang (University of Western Ontario) and Fred Pearson (McMaster University) for their kind help of HRTEM.

References

[1] K. Kordesch, G. Simander, Fuel Cells and their Applications, VCH, Germany, 1996, 73 pp.
[2] K. Lee, J. Zhang, H. Wang, D.P. Wilkinson, J. Appl. Electrochem. 36 (2006) 507–522.
[3] H.A. Gasteiger, S.S. Kocha, B. Sompalli, F.T. Wagner, Appl. Catal. B: Environ. 56 (2005) 9–35.
[4] H.-F. Oetjen, V.M. Schmidt, U. Stimming, F. Trila, J. Electrochem. Soc. 143 (1996) 3838–38841.
[5] T. He, E. Kreidler, L. Xiong, J. Luo, C.J. Zhong, J. Electrochem. Soc. 153 (2006) A1637–A1639.
[6] H.A. Gasteiger, J.E. Panels, S.G. Yan, J. Power Sources 127 (2004) 162–171.
[7] R. Borup, J. Meyers, B. Pivovar, Y.S. Kim, R. Mukundan, N. Garland, D. Myers, M. Wilson, F. Garzon, D. Wood, P. Zelenay, K. More, K. Stroh, T. Zawodzinski, J. Boncella, J.E. McGrath, M. Inaba, K. Miyatake, M. Hori, K. Ota, Z. Ogumi, S. Miyata, A. Nishikata, Z. Siroma, Y. Uchimoto, K. Yasuda, K.-I. Kimijima, N. Iwashita, Chem. Rev. 107 (2007) 3904–3951.
[8] C. Bock, C. Paquet, M. Couillard, G.A. Botton, B.R. MacDougall, J. Am. Chem. Soc. 126 (2004) 8028–8037.
[9] R.H. Baughman, A.A. Zakhidov, W.A. Heer, Science 297 (2002) 787–792.
[10] W. Li, C. Liang, W. Zhou, J. Qiu, Z. Zhou, G. Sun, Q. Xin, J. Phys. Chem. B 107 (2003) 6292–6299.
[11] N. Rajalakshmi, H. Ryu, M.M. Shaijumon, S. Ramaprabhu, J. Power Sources 140 (2005) 250–257.
[12] G. Girishkumar, K. Vinodgopal, P.V. Kamat, J. Phys. Chem. B 108 (2004) 19960–19966.
[13] E.S. Steigerwalt, G.A. Deluga, C.M. Lukehart, J. Phys. Chem. B 106 (2002) 760–766.
[14] Y. Shao, G. Yin, Y. Gao, J. Power Sources 171 (2007) 558–566.
[15] Y. Shao, G. Yin, J. Wang, Y. Gao, P. Shi, J. Power Sources 161 (2006) 47–53.
[16] H.J. Zheng, C.N. Ma, W. Wang, J.G. Huang, Electrochem. Commun. 8 (2006) 977–981.
[17] C.L. Guo, Y. Liu, X.J. Ma, Y.T. Qian, L.Q. Xu, Chem. Lett. 35 (2006) 1210–1211.
[18] Y. Shao, G. Yin, Y. Gao, P. Shi, J. Electrochem. Soc. 153 (2006) A1093–A1097.
[19] M.S. Saha, R. Li, X. Sun, J. Power Sources 177 (2008) 314–322.
[20] M.M. Waje, X. Wang, W. Li, Y. Yan, Nanotechnology 16 (2005) 395–400.
[21] X. Wang, M. Waje, Y. Yan, Electrochem. Solid-State Lett. 8 (2005) A42–A44.
[22] D. Villers, S.H. Sun, A.M. Serventi, J.P. Dodelet, J. Phys. Chem. B 110 (2006) 25916–25925.
[23] X. Sun, R. Li, D. Villers, J.P. Dodelet, S. Desilets, Chem. Phys. Lett. 379 (2003) 99–104.
[24] M.S. Saha, Y. Chen, R. Li, X. Sun, Asia-Pacific J. Chem. Eng. in press.
[25] B. Wu, A. Heidelberg, J.J. Boland, Nat. Mater. 4 (2005) 525–529.
[26] A.S. Edelstein, R.C. Cammarata (Eds.), Nanomaterials: Synthesis, Properties and Applications, Inst Phys, Bristol, UK, 1996, pp. 596.
[27] H.S. Nalwa, Handbook of Nanostructured Materials and Nanotechnology, in: Synthesis and Processing, vol.1, Academic, San Diego, Calif, 2000, pp. 645.
[28] Y. Xia, P. Yang, Y. Sun, Y. Wu, B. Mayers, B. Gates, Y. Yin, F. Kim, H. Yan, Adv. Mater. 15 (2003) 353–389 (Weinheim, Germany).
[29] L. Jiang, G. Sun, Z. Zhou, S. Sun, Q. Wang, S. Yan, H. Li, J. Tian, J. Guo, B. Zhou, Q. Xin, J. Phys. Chem. B 109 (2005) 8774–8778.
[30] A.L. Santos, D. Profeti, P. Olivi, Electrochim. Acta 50 (2005) 2615–2621.
[31] T. Okanishi, T. Matsui, T. Takeguchi, R. Kikuchi, K. Eguchi, Appl. Catal. A: Gen. 298 (2006) 181–187.
[32] M.S. Saha, R. Li, M. Cai, X. Sun, Electrochem. Solid-State Lett. 10 (2007) B130–B133.
[33] M.S. Saha, R. Li, X. Sun, Electrochem. Commun. 9 (2007) 2229–2234.
[34] L. Jankovic, D. Gournis, P.N. Trikalitis, I. Arfaoui, T. Cren, P. Rudolf, M.-H. Sage, T.T.M. Palstra, B. Kooi, J.D. Hosson, M.A. Karakassides, K. Dimos, A. Moukarika, T. Bakas, Nano Lett. 6 (2006) 1131–1135.
[35] Y. Jiang, X.M. Meng, J. Liu, Z.R. Hong, C.S. Lee, S.T. Lee, Adv. Mater. 15 (2003) 1195–1198.
[36] I. Grigoriants, A. Soffer, G. Salitra, D. Aurbach, J. Power Sources 146 (2005) 185–189.
[37] T. Morishita, T. Hirabayashi, T. Okuni, N. Ota, M. Inagaki, J. Power Sources 160 (2006) 638–642.
[38] J. Read, D. Foster, J. Wolfenstine, W. Behl, J. Power Sources 96 (2001) 277–281.
[39] R. Li, X. Sun, X. Zhou, M. Cai, X. Sun, J. Phys. Chem. C 111 (2007) 9130–9135.
[40] A.M. Kannan, V.P. Veedu, L. Munukutla, M.N. Ghasemi-Nejhad, Electrochem. Solid-State Lett. 10 (2007) B47–B50.

[41] A.J. Bard, L.R. Faulkner, Electrochemical Methods, Fundamentals and Applications, Wiley, New York, 1980.
[42] E.M. Crabb, R. Marshall, D. Thompsett, J. Electrochem. Soc. 147 (2000) 4440–4447.
[43] K. Wang, H.A. Gasteiger, N.M. Markovic, P.N. Ross, Electrochim. Acta 41 (1996) 2587–2593.
[44] A.J. Dickinson, L.P.L. Carrette, J.A. Collins, K.A. Friedrich, U. Stimming, Electrochim. Acta 47 (2002) 3733–3739.
[45] M. Go¨tz, H. Wendt, Electrochim. Acta 43 (1998) 3637–3644.
[46] M. Watanabe, S. Motoo, Electroanal. Chem. Interf. Electrochem. 60 (1975) 267–273.
[47] C. Bock, M.-A. Blakely, B. MacDougall, Electrochim. Acta 50 (2005) 2401–2414.